Estimation of Uncompensated Trajectory Deviations and Image Refocusing for High-Resolution SAR

Ievgen M. Gorovyi, Oleksandr O. Bezvesilniy and Dmytro M. Vavriv
Department of Microwave Electronics, Institute of Radio Astronomy of NAS of Ukraine
4 Chervonopraporna Str., Kharkov 61002, Ukraine
gorovoy@rian.kharkov.ua, obezv@rian.kharkov.ua, vavriv@rian.kharkov.ua

Abstract— **The accuracy of trajectory measurements is one of the crucial factors in high-resolution SAR imaging. Common navigation systems often do not fulfill the requirements that results in significant image quality degradation. In the paper, a new autofocus algorithm for the reconstruction of the SAR platform trajectory deviations is proposed. The approach is based on the estimation of the Doppler rate errors on a sequence of short-time intervals. The method is capable of estimation of time-varying and range-dependent phase error functions. The key steps of the developed technique are illustrated. The method is demonstrated on experimental data obtained with an X-band airborne SAR system.**

Keywords—synthetic aperture radar; autofocus; phase errors; residual trajectory deviations

I. INTRODUCTION

Synthetic aperture radar (SAR) is a well-known instrument for high-resolution imaging of the Earth surface [1]-[3]. The quality of obtained images strongly depends on the precision of SAR platform trajectory measurements [1], [4]-[7]. The problem is that the navigation systems have a limited precision and often do not fulfill the existing requirements. This results in uncompensated residual trajectory deviations, which lead to a significant SAR image quality degradation [2], [4].

In order to compensate the residual trajectory deviations, autofocus techniques are commonly applied [1]-[3]. The challenge is that there is no a universal autofocus algorithm. Some methods require the existence of bright targets on a scene, while other techniques are based on different analytical models for the residual phase error function.

Recently a novel autofocus method called local-quadratic map-drift autofocus (LQMDA) was developed [8]. The approach is based on the estimation of local-quadratic phase errors on short-time intervals which are used for an arbitrary phase error reconstruction.

The problem is that the residual phase errors can demonstrate considerable range dependence as the projection of the trajectory deviations on the radial direction considerably changes across the swath. Such range dependence should be carefully accounted. In the paper, we propose several important ideas that allow to improve the efficiency of the residual phase error estimation and successfully account its range dependence.

In Section II, peculiarities of the SAR image formation on a short-time interval and ideas of the local quadratic phase error estimation are described. Important SAR image pre-processing steps that are applied before the cross-correlation calculation are introduced in Section III. An efficient trajectory restoration scheme with specifically chosen weighting coefficients is also described in this section. In Section IV, practical results of the application of the autofocus technique to the real SAR data obtained with an X-band airborne SAR system are provided.

II. SAR PROCESSING AND LOCAL PHASE ERROR ESTIMATION ON A SHORT-TIME INTERVAL

Generally, the residual uncompensated phase error $\varphi_E(R,t)$ in the backscattered radar signal is an arbitrary function. In airborne SAR systems, low-frequency phase errors are more critical [2], while the impact of fast-varying phase errors can be neglected in many cases. Recently, it has been shown that the phase error function can be efficiently described by using the local approximation principle [4]. According to this idea, the phase error on a short-time interval at a range gate R can be described in the following way:

$$\varphi_E(R,t_n+\tau) \approx \varphi_E(R,t_n) + \varphi'_E(R,t_n)\tau + \varphi''_E(R,t_n)\tau^2/2, \quad (1)$$

where t_n is the center of the considered short-time interval of duration T_S, τ is the time within the short interval, $-T_S/2 < \tau < T_S/2$. In the approximation (1), the linear phase term $\varphi'_E(R,t_n)\tau$ causes the shift of the SAR image in the azimuth direction, while the quadratic phase error term $\varphi''_E(R,t_n)\tau^2/2$ leads to the image defocusing. Since the final SAR image represents only the intensity, the constant phase term $\varphi_E(R,t_n)$ can be neglected. The length of the short-time intervals can be chosen to provide the sufficient precision of the local phase error approximation [8].

The key thing is that the local quadratic phase error $\varphi''_E(R,t_n)$ can be estimated with the map-drift principle via the formation of a pair of SAR images from two halves of a short-time interval [8]. For the formation of such images, a specifically modified version of the range-Doppler algorithm [9] can be used.

Another option for the SAR synthesis on a short-time interval is the dechirp algorithm [2]. In this case, the computation burden can be significantly reduced and each of the SAR images can be obtained using a single short Fourier transform:

$$I_1(R,f)=\frac{2}{T_S}\int_{-T_S/2}^{0} w_S(\tau+T_S/4)s(R,\tau)h^*(R,\tau)\exp[-2\pi i f\tau]d\tau,$$

$$I_2(R,f)=\frac{2}{T_S}\int_{0}^{T_S/2} w_S(\tau-T_S/4)s(R,\tau)h^*(R,\tau)\exp[-2\pi i f\tau]d\tau.$$

Here f is the azimuth spatial frequency, $s(R,\tau)$ is a backscattered signal, $w_S(\tau)$ is a weighting window, $h(R,\tau)$ is a time-domain reference function,

$$h(R,\tau)=\exp[2\pi i(F_{DC}(R)\tau+F_{DR}(R)\tau^2/2)],$$

where F_{DC} and F_{DR} are the known Doppler centroid and Doppler rate calculated from the navigation data. The frequency f is related to the azimuth coordinate X as $f=-F_{DR}X/V$, where V is the speed of the SAR platform.

In the presence of the local quadratic phase error, the SAR images will be defocused and shifted in the azimuth in the opposite directions [8]. One can show that the value of this shift determines the Doppler rate error F_{DR}^E on the short-time interval:

$$\Delta f_{\max}=f_{1\max}-f_{2\max}=F_{DR}^E T_S/2. \qquad (2)$$

The linear shift (2) can be measured via the calculation of the cross-correlation of the two SAR images. The aim is to provide a very precise estimation of the position of the cross-correlation peak.

III. SAR Image Cross-Correlation and Trajectory Estimation Procedures

A. Pre-processing Steps for Image Shift Estimation

The problem is that the direct calculation of the images cross-correlation can often lead to inaccurate results. For example, artificial targets on the scene may lead to correlation functions with multiple peaks; the presence of large-scale objects may broaden the cross-correlation maxima significantly etc. In order to estimate the position of the correlation maxima more reliably and accurately, several pre-processing steps are proposed to be applied to the SAR images before the calculation of the cross-correlation functions.

It is known that SAR images typically have a high dynamic range that is the radar cross section (RCS) changes significantly over the scene. Therefore SAR images are typically displayed in a logarithmic scale. In order to balance the contributions to the correlation maxima from bright targets as compared to the other elements of the ground scene, the logarithmic representation of SAR images should also be used during the correlation calculation. Additionally, the limitation of the image dynamic range is to be performed as follows:

$$I_{\mathrm{LDR}}(R_n,X_k)=\begin{cases} T_{\mathrm{dB}}^{\mathrm{U}}, & \text{if } I_{\mathrm{dB}}(R_n,X_k)>T_{\mathrm{dB}}^{\mathrm{U}},\\ I_{\mathrm{dB}}(R_n,X_k), & \text{if } T_{\mathrm{dB}}^{\mathrm{L}}\le I_{\mathrm{dB}}(R_n,X_k)\le T_{\mathrm{dB}}^{\mathrm{U}},\\ T_{\mathrm{dB}}^{\mathrm{L}}, & \text{if } I_{\mathrm{dB}}(R_n,X_k)<T_{\mathrm{dB}}^{\mathrm{L}}, \end{cases}$$

where $I_{\mathrm{dB}}(R_n,X_k)$ is the image in a logarithmic scale, and $I_{\mathrm{LDR}}(R_n,X_k)$ is the image with the limited dynamic range. The upper threshold $T_{\mathrm{dB}}^{\mathrm{U}}$ limits the values of bright targets; the lower threshold $T_{\mathrm{dB}}^{\mathrm{L}}$ restricts the values of radio shadows and not illuminated areas outside the antenna footprint.

In order to solve the problem of strong influence of large-scale objects with complex geometric shapes (such as rivers, lakes, forest areas, etc.), a local centering is applied to the SAR images before the shift measurements. Such procedure is accomplished in two steps. First, the local smoothing of the image is performed:

$$I_{\mathrm{SM}}(R_n,X_k)=\sum_{p=-P}^{P}\sum_{q=-Q}^{Q} W_{\mathrm{SM}}(p,q)I_{\mathrm{LDR}}(R_{n+p},X_{k+q}),$$

where $W_{\mathrm{SM}}(p,q)$ is the aperture window of the smoothing filter. Second, the locally centered image is calculated:

$$I_{\mathrm{LC}}(R_n,X_k)=I_{\mathrm{LDR}}(R_n,X_k)-I_{\mathrm{SM}}(R_n,X_k).$$

The obtained images after the described preprocessing steps are used for the cross-correlation calculations. For a particular range gate, it is determined as

$$R_{CC}(R,\Delta X)=\int |I_{LC1}(R,X)|^2\,|I_{LC2}(R,X+\Delta X)|^2\,dX.$$

The application of the described dynamic range limitation and local centering leads to sharp correlation peaks and more reliable shift estimations.

B. Trajectory Estimation Procedure

An additional challenge for SAR autofocusing is the accounting for the range dependence of the phase error. This is especially important for wide-range-swath and low-altitude SAR systems. To solve the problem, we have developed an approach, which derives uncompensated trajectory deviations from the local Doppler rate error estimates.

From the SAR geometry, one can show that the Doppler rate of the backscattered signal is determined as follows:

$$F_{DR}(R,t_n)=$$
$$=-\frac{2}{\lambda}\left[\frac{1}{R}\left(\left|\vec{V}+\vec{v}_E(t_n)\right|^2-\left(\frac{\vec{R}\cdot\left(\vec{V}+\vec{v}_E(t_n)\right)}{R}\right)^2\right)-\frac{\vec{R}\cdot\vec{a}_E(t_n)}{R}\right],$$

where $\vec{V}$ is the reference velocity vector, $\vec{v}_E(t_n)$ is the velocity error vector, $\vec{a}_E(t_n)$ is the acceleration error vector, and $\vec{R}$ is the slant range vector.

It has been found that the main contribution to the phase errors comes from with the cross-track acceleration components $a_Y(t_n), a_Z(t_n)$. Thus, the estimated Doppler rate error can be written as

$$F_{DR}^E(R,t_n)\approx\frac{2}{\lambda}\frac{y_R a_Y(t_n)-Ha_Z(t_n)}{R}, \qquad (3)$$

where $y_R = -H\tan\alpha\sin\beta + \cos\beta\sqrt{R^2 - H^2 - (H\tan\alpha)^2}$, R is the slant range, H is the flight altitude, α, β are the antenna pitch and yaw angles, respectively.

The expression (3) can be used for the estimation of the cross-track acceleration components. For this purpose, one can construct the mean square estimator (MSE) based on the Doppler rate errors estimated within several range blocks:

$$MSE(a_Y(t_n), a_Z(t_n)) = \\ = \sum_{m=1}^{M_R} w_m(t_n)\left[\frac{2}{\lambda}\frac{y_{R_m}a_Y(t_n) - Ha_Z(t_n)}{R_m} - F_{DR}^E(R_m, t_n)\right]^2, \quad (4)$$

where R_m is the central range gate of each range block, and $F_{DR}^E(R_m, t_n)$ are the estimated Doppler rate errors.

The weighting coefficients $w_m(t_n)$ are the values of the cross-correlation functions maxima. Such choice can be easily explained. The value of the cross-correlation peak is proportional to the image contrast. Evidently, the peak position estimation is more accurate and reliable for range blocks with a higher contrast. Therefore, the usage of such weighting allows balancing the contributions from image areas with different contrast.

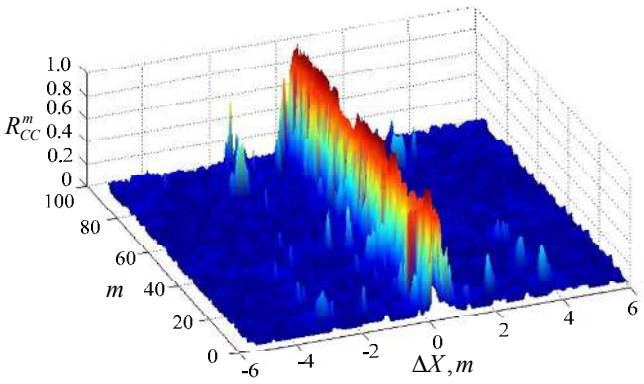

Figure 1. Cross-correlation functions for different range blocks.

An example of the local correlation functions $R_{CC}^m(m, \Delta X)$ for a set of range blocks is illustrated in Fig. 1. One can see that the maximum values of the cross-correlation peak are different for different range blocks. The cross-correlation function for each range block m is calculated as an average of cross-correlation functions $R_{CC}(R_n, \Delta X)$ for all range gates within this block:

$$R_{CC}^m(m, \Delta X) = \frac{1}{N_{RB}}\sum_{n=0}^{N_{RB}-1} R_{CC}(R_{mN_{RB}+n}, \Delta X).$$

Since the speckle noise from different range bins is uncorrelated, such averaging leads to the noise variance reduction in $\sqrt{N_{RB}}$ times.

An example of the calculated cross-correlation maxima values $w_m(m, t_n)$ for different range blocks and azimuth positions is illustrated in Fig. 2. One can see that the values of the cross-correlation maxima change significantly, and such behavior is accounted in the weighting scheme (4).

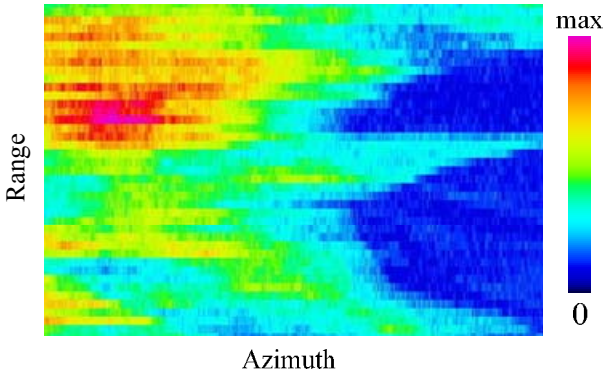

Figure 2. Example of calculated weighting coefficients.

From (4) one can derive the system of equations for the unknown cross-track acceleration components:

$$a_Y(t_n)\sum_{m=1}^{M_R} w_m\left(\frac{y_{R_m}}{R_m}\right)^2 - a_Z(t_n)\sum_{m=1}^{M_R} w_m\left(\frac{y_{R_m}}{R_m}\frac{H}{R_m}\right) = \\ = \frac{\lambda}{2}\sum_{m=1}^{M_R} w_m F_{DR}^E(R_m, t_n)\frac{y_{R_m}}{R_m},$$

$$a_Y(t_n)\sum_{m=1}^{M_R} w_m\left(\frac{y_{R_m}}{R_m}\frac{H}{R_m}\right) - a_Z(t_n)\sum_{m=1}^{M_R} w_m\left(\frac{H}{R_m}\right)^2 = \\ = \frac{\lambda}{2}\sum_{m=1}^{M_R} w_m F_{DR}^E(R_m, t_n)\frac{H}{R_m}.$$

In this way, the uncompensated cross-track acceleration components $a_Y(t_n), a_Z(t_n)$ are found. At the next step, the trajectory deviations are evaluated by double integration and used for the calculation of the range-dependent phase error functions. Finally, these phase errors are to be compensated properly in the SAR data.

IV. Experimental Results

Based on the introduced ideas, a novel autofocus approach has been developed. The input for the proposed method is the SAR data after the range compression, the range cell migration correction and the conventional motion compensation procedure based on the measured navigation data [2]-[4]. After these initial steps the radar data is ready for the application of the developed autofocus method.

The main stages of the proposed algorithm are shown in Fig. 3. At the first step, the data are divided on small azimuth blocks. Then, the pairs of SAR images are built on the corresponding short-time intervals. After that, the Doppler rate errors $F_{DR}^E(R_m, t_n)$ is estimated using the developed linear shift estimation procedure.

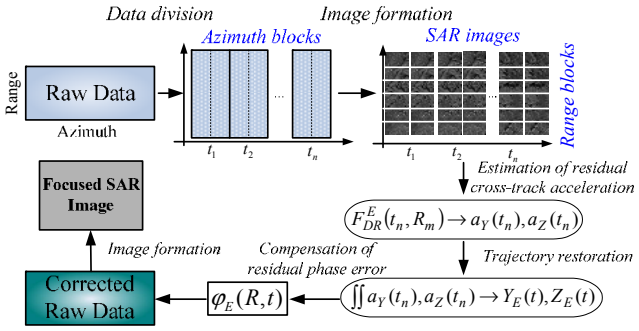

Figure 3. Block-scheme of the proposed algorithm.

The obtained Doppler rate errors are used for the reconstruction of the residual trajectory deviations via the proposed weighted estimation scheme. At the final step, the range-dependent residual phase error functions are calculated and compensated in the SAR data.

The developed autofocus method has been successfully tested with the airborne RIAN-SAR-X system [10] developed and produced at the Institute of Radio Astronomy of the National Academy of Sciences of Ukraine. An example of multi-look SAR image obtained without autofocusing is shown in Fig. 4(a). Evidently, this image is significantly defocused. Such defocusing is caused by uncompensated platform deviations. The SAR image of the same scene after the application of the developed autofocus method is shown in Fig. 4(b). This image is well focused that confirms the efficiency of the proposed approach.

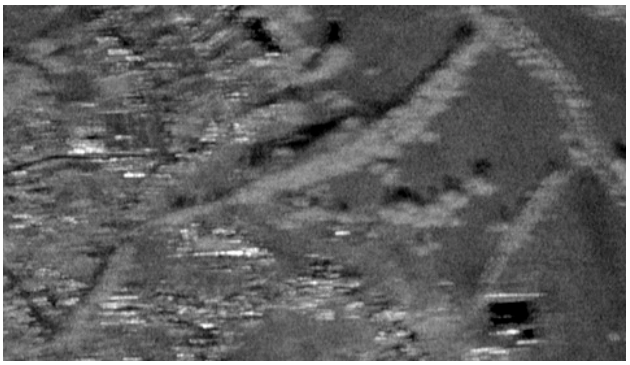

(a)

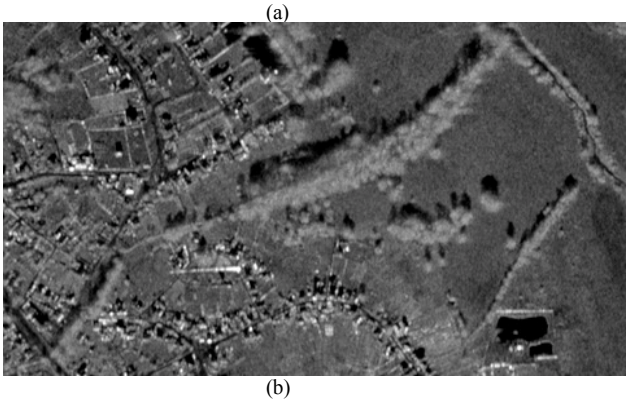

(b)

Figure 4. Multi-look SAR images (25 looks, 2-m resolution): (a) – before autofocusing, (b) – after autofocusing.

V. Conclusion

In the paper, a new approach for the reconstruction of the residual uncompensated SAR platform trajectory deviations is proposed. The method is based on the estimation of the Doppler rate errors on short-time intervals with the consequent estimation of the cross-track acceleration components. Several important pre-processing steps are introduced that allows to significantly improve the precision of the estimation. It has been shown that the developed method can successfully handle both time-varying and range-dependent phase errors. The efficiency of the method has been confirmed on practice with airborne SAR data.

References

[1] C. Oliver and S. Quegan, Understanding Synthetic Aperture Radar Images. Norwood, MA: Artech House, 1999.

[2] W. G. Carrara, R. S. Goodman, and R. M. Majewski, Spotlight Synthetic Aperture Radar: Signal Processing Algorithms. Boston; London: Artech House, 1995.

[3] I. G. Cumming and F. H. Wong, Digital Processing of Synthetic Aperture Radar Data: Algorithms and Implementation". Norwood, MA: Artech House, 2005.

[4] O.O. Bezvesilniy, I.M. Gorovyi and D.M. Vavriv, "Effects of local phase errors in multi-look SAR images", Progress In Electromagnetics Research B, Vol. 53, pp.1-24, 2013.

[5] K. A. C. de Macedo et al, "Precise topography- and aperture-dependent motion compensation for airborne SAR", IEEE Geosci. Remote Sens. Lett., Vol. 2, No. 2, pp. 172–176, 2005.

[6] P. Prats et al., "Comparison of topography and aperture dependent motion compensation algorithms for airborne SAR", IEEE Geosci. Remote Sens. Lett., Vol. 4, No. 3, pp. 349–353, 2007.

[7] A. Reigber et al., "Very-High-Resolution Airborne Synthetic Aperture Radar Imaging: Signal Processing and Applications", Proceedings of the IEEE, Vol. 101, No. 3, 2013.

[8] O.O. Bezvesilniy, I.M. Gorovyi and D.M. Vavriv, "Estimation of phase errors in SAR data by local-quadratic map-drift autofocus", Proc. 13th Int. Radar Symp. IRS-2012, Warsaw, Poland, pp. 376-381, 2012.

[9] I.M. Gorovyi, O.O. Bezvesilniy and D.M. Vavriv, "Modifications of Range-Doppler Algorithm for Compensation of SAR Platform Motion Instabilities", International Journal of Electronics and Telecommunications, Vol. 60, no. 3, pp.225-231, 2014.

[10] D. M. Vavriv at al., "X-band SAR system for light-weight Aircrafts", Proc. 15th Int. Radar Symp. IRS-2014, Gdansk, Poland, pp. 501–505, 2014.

ISBN 978-3-9812668-6-3